HAL
open science

Structural insight into the role of the Ton complex in energy transduction

Hervé H. Celia, Nicholas Noinaj, Stanislav D Zakharov, Enrica Bordignon, Istvan Botos, Mónica Santamaria, Travis J Barnard, William A Cramer, Roland Lloubès, Susan K Buchanan

To cite this version:

Hervé H. Celia, Nicholas Noinaj, Stanislav D Zakharov, Enrica Bordignon, Istvan Botos, et al.. Structural insight into the role of the Ton complex in energy transduction. Nature, 2016, 538 (7623), pp.60 - 65. 10.1038/nature19757 . hal-01788473

HAL Id: hal-01788473

https://amu.hal.science/hal-01788473

Submitted on 9 May 2018

HAL is a multi-disciplinary open access archive for the deposit and dissemination of scientific research documents, whether they are published or not. The documents may come from teaching and research institutions in France or abroad, or from public or private research centers.

L'archive ouverte pluridisciplinaire **HAL**, est destinée au dépôt et à la diffusion de documents scientifiques de niveau recherche, publiés ou non, émanant des établissements d'enseignement et de recherche français ou étrangers, des laboratoires publics ou privés.

Structural insight into the role of the Ton complex in energy transduction

Hervé Celia[1,5¥], Nicholas Noinaj[2¥*], Stanislav D. Zakharov[2], Enrica Bordignon[3,4], Istvan Botos[5], Monica Santamaria[6], Travis J. Barnard[5], William A. Cramer[2], Roland Lloubes[1*], and Susan K. Buchanan[5*]

[1]Laboratoire d'Ingénierie des Systèmes Macromoléculaires, UMR7255 CNRS/Aix-Marseille Université, Institut de Microbiologie de la Méditerranée, 13402 Marseille Cedex 20, France, [2]Markey Center for Structural Biology, Department of Biological Sciences, Purdue University, West Lafayette, Indiana, 47907, [3]Fachbereich Physik, Freie Universität, 14195 Berlin, Germany, [4]Faculty of Chemistry and Biochemistry, Ruhr-Universität Bochum, 45810 Bochum, Germany, 5, National Institute of Diabetes & Digestive & Kidney Diseases, Bethesda, Maryland, 20892, and [6]Departamento de Cirugia Experimental, Instituto de Investigacion Hospital La Paz (IdiPAZ), Paseo de la Castellana 261, 28046 Madrid, Spain

[¥]Authors contributed equally.

*For correspondence: skbuchan@helix.nih.gov; nnoinaj@purdue.edu; lloubes@imm.cnrs.fr

Running Title: The crystal structure of the Ton subcomplex

Summary

In Gram-negative bacteria, outer membrane (OM) transporters import nutrients by coupling to an inner membrane (IM) protein complex called the Ton complex. The Ton complex consists of TonB, ExbB, and ExbD, and uses the proton motive force (pmf) at the IM to transduce energy to the OM via TonB. The mechanism and stoichiometry of the complex have remained unknown. Here, we structurally characterize the Ton subcomplex (ExbB/ExbD) from *E. coli* using X-ray crystallography, electron microscopy, DEER spectroscopy, and crosslinking, revealing that ExbB assembles as a pentamer containing a transmembrane pore filled by a single ExbD that is dimerized to a second ExbD sitting outside of the pore. Combined with our studies using the fully assembled Ton complex, we report a stoichiometry consisting of a pentamer of ExbB, a dimer of ExbD, and at least one TonB. Electrophysiology studies show that the Ton subcomplex forms pH-sensitive cation-selective channels, providing insight to the mechanism by which it may harness the pmf for energy production.

Introduction

Gram-negative bacteria contain a double membrane system that serves as a barrier to large toxic molecules, while allowing import of essential nutrients. Although transport across a membrane typically requires an energy source, there is no known energy source located in the outer membrane (OM). To overcome this deficiency, bacteria have evolved systems to harness the energy produced from the proton motive force (pmf) generated at the inner membrane (IM) and transduce it for transport at the OM[1,2]. An example is the Ton system that mediates the uptake of metals, carbohydrates, iron-siderophore complexes, cobalamin, and many bacteriocins[3-6]. The Ton system consists of (i) the energy transducing Ton complex located within the IM and (ii) the ligand-specific TonB-dependent (TBD) transporter found within the OM, which interacts with the ligands to be transported[2,7-9] **(**Fig. 1a). The Ton complex is formed by three integral polytopic membrane proteins ExbB, ExbD, and TonB, which together transduce the energy stored

45 in the pmf at the IM to the TBD transporters at the OM. The energy transfer is mediated by a conserved 5-7
46 residue TonB-box at the N-terminus of all TBD transporters[2,10]. Upon ligand binding to the TBD
47 transporter, the TonB box becomes exposed and the interaction with TonB leads to conformational changes
48 in the TBD transporter that are coupled to ligand transport across the OM. Due to the lack of sufficient
49 structural information, the detailed mechanism by which energy is transduced from the IM to the OM by
50 the Ton complex is unknown.

51 ExbB is predicted to contain three transmembrane spanning helices (TMHs) with a large
52 cytoplasmic domain, whereas ExbD and TonB are each predicted to contain a single N-terminal TMH that
53 anchors a large C-terminal periplasmic domain in the IM[11-15] (Fig. 1a). The exact stoichiometry of
54 components of the Ton complex has been a matter of debate for many years. Depending upon the methods
55 of analysis, the ExbB/ExbD/TonB ratio within the complete Ton complex has been reported to be 7:2:1 and
56 4:1:1, and for the ExbB/ExbD subcomplex 4:2 and 6:1[16-19]. Recent studies have suggested that in the
57 absence of TonB, the subcomplex contains two ExbD molecules; however, the association of TonB with
58 the complex displaces one copy of ExbD, such that a single ExbD molecule is left in the fully assembled
59 Ton complex[17]. Evidence favoring a dynamic mechanism has been reported in which fluorescence
60 anisotropy studies showed that the presence of TonB within the Ton complex sustains a rotational motion
61 dependent on the pmf at the IM[20].

62 The Ton complex is often compared to the Tol complex, which consists of the analogous
63 components TolQ, TolR, and TolA, with each component sharing both sequence and structure conservation
64 including the topology of the TM domains[21,22]. The Tol complex is required for cell envelope integrity[23,24]
65 and to maintain cellular structure during cell division[25]. And similar to TonB for the Ton system, energy
66 dependent conformational changes have been demonstrated for TolA as well[20,26,27]. The Ton complex is
67 also evolutionarily related to the Mot complex, which drives bacterial flagellar motion[22,28-30]. Here, MotA
68 and MotB work in concert to convert energy from the pmf into a motor-like mechanical energy that powers

motility of bacteria via their flagella. Knowing how the Ton complex functions will also assist in elucidating the functions of both the Tol and Mot complexes.

To better understand the role of the Ton complex in energy transduction to the OM, we solved crystal structures of the *E. coli* Ton subcomplex consisting of full-length ExbB and a truncated construct of ExbD. We further characterized the assembly of the subcomplex using electron microscopy, crosslinking, and DEER spectroscopy, which reveal that ExbB assembles as a pentamer containing a transmembrane pore filled by a single ExbD that is dimerized to a second ExbD sitting outside of the pore. No change in stoichiometry was observed in the presence of TonB as observed by SDS-PAGE analysis and DEER spectroscopy, confirming that the fully assembled Ton complex consists of a pentamer of ExbB, a dimer of ExbD, and at least one TonB. Using electrophysiology, we also show that the Ton subcomplex forms pH-sensitive cation-selective channels, suggesting a mechanism by which it can harness the pmf for energy transduction.

Results

The crystal structure of the Ton subcomplex

The various constructs of the Ton subcomplex (ExbB/ExbD) were co-expressed in either BL21(DE3) or B834 cells, solubilized directly from membranes, and purified by a C-terminal 6x-His tag on ExbD. For tag removal, the sample was treated with TEV protease and then detergent-exchanged using size exclusion chromatography (SEC) (Fig. 1b, c). For crystallization, the samples were methylated prior to performing crystallization trials. Native crystals of the Ton subcomplex lacking the periplasmic domain of ExbD (ExbB/ExbD$_{\Delta peri}$) were grown by vapor diffusion from well solutions containing either (*i*) 100 mM HEPES-NaOH, pH 7.0, 100 mM $CaCl_2$, and 22% PEGMME 550 or (*ii*) 100 mM Na-acetate, pH 4.5, 100 mM $MgCl_2$, and 25% PEG 400. For structure determination, selenomethionine-substituted protein produced crystals in 100 mM MES/imidazole, pH 6.5, 30 mM $MgCl_2$, 30 mM $CaCl_2$, 50% ethylene glycol,

93 and 8% PEG 8000. The initial phases were calculated using a 5.2 Å Se-SAD dataset of ExbB/ExbD$_{\Delta peri}$,
94 which produced an interpretable electron density map allowing an initial poly-alanine model to be built
95 (Supplementary Fig. 1). This starting model was then used to solve crystal structures of the ExbB/ExbD$_{\Delta peri}$
96 complex at pH 4.5 and 7.0 by molecular replacement (Supplementary Table 1).

97 The structure of the ExbB/ExbD$_{\Delta peri}$ complex at pH 7.0 was solved to 2.6 Å resolution. However,
98 only ExbB could be built due to insufficient density for ExbD$_{\Delta peri}$ (Supplementary Figs 2 and 3). In this
99 structure, the ExbB monomer adopts an extended conformation sitting perpendicular to the membrane,
100 consisting of seven α-helices with α2 and α7 measuring 80-100 Å in length and α5 and α6 forming an
101 extended helix (~100 Å) separated by a kink (Fig. 1d). The N-terminal region of ExbB is mostly disordered
102 before residue Ser11 where α1 resides parallel to the membrane, a conformation possibly used to help
103 stabilize the complex within the membrane. The TM domain consists of three transmembrane helices
104 formed by α2, α6, and α7 while the remainder of the helices compose the cytoplasmic domain consisting
105 of cytoplasmic domain 1 and the C-terminal domain, forming a 5-helix bundle.

106 The quaternary structure of ExbB is a pentamer where the five TM domains come together to form
107 a transmembrane pore (α6 and α7), while the cytoplasmic domains form a large enclosed cavity extending
108 as far as ~60 Å into the cytoplasm (Fig. 1e, f, g). The cytoplasmic domain of ExbB retains 5-fold symmetry
109 with each edge measuring ~45 Å, while the periplasmic domain is arranged in pseudo 5-fold symmetry
110 with each edge measuring ~35 Å. ExbB forms a large extended cavity (largest pore radius ~11 Å) along the
111 cytoplasmic and TM domains which is open, yet constricted on each end (pore radius ~2 Å on the
112 cytoplasmic side and ~4 Å along the TM side) (Fig. 1h). Each monomer has ~3,000 Å^2 of buried surface
113 area with the two adjacent molecules (~20% of total surface area), indicating a stable oligomeric state. For
114 the cytoplasmic cavity, five side fenestrations are observed which could allow solvent or ion passage (Fig.
115 1h, i). Sparse electron density indicated that the TM pore of ExbB is likely filled by the TMH of ExbD$_{\Delta peri}$;
116 however, this density was too diffuse to allow a model to be built unambiguously (Supplementary Fig. 3).
117 Two ExbB pentamers were observed per asymmetric unit and alignment of these pentamers reveals some

118 helical shifts, possibly indicating a propensity for movement within the membrane domain (Supplementary
119 Fig. 4). The B-factors along the cytoplasmic domain indicate that this is the most ordered region of the
120 structure, suggesting little flexibility (Supplementary Fig. 5).

121 To verify the presence of the TMH of $ExbD_{\Delta peri}$ within the TM pore of the ExbB pentamer, we
122 solved the structure of $ExbB/ExbD_{\Delta peri}$ at pH 4.5, to 3.5 Å resolution and observed a single α-helix (Fig. 2a,
123 b, Supplementary Table 1, Supplementary Fig. 6, and Supplementary Movie 1). From the density, an
124 extended α-helix could be built consisting of residues 22-45, which correlated well with the hydrophobic
125 residues inside the TM pore of ExbB, although, it was offset by ~10 Å from the position of the TM
126 domains of ExbB predicted to be embedded into the membrane. The exact position of each residue was less
127 precise due to the lack of well-defined side chain density. Due to the size of the TM pore of ExbB, only one
128 α-helix can be accommodated within it, albeit relatively loosely, which may allow it to move rotationally
129 and/or translationally. In the $ExbB/ExbD_{\Delta peri}$ complex structure solved at pH 7.0, little to no density for the
130 TMH of $ExbD_{\Delta peri}$ was observed; however, for the structure solved at pH 4.5, the TMH was clearly
131 observed (Supplementary Fig. 7). This suggests that movements of the TMH of $ExbD_{\Delta peri}$ within the TM
132 pore of ExbB may be modulated by the change in pH, which may be a clue to the mechanism by which the
133 Ton complex responds to the pmf across the inner membrane.

134 A striking feature of the ExbB pentamer is the very large cytoplasmic domain and its electrostatic
135 properties, which includes a strongly electropositive 'basic belt' that sits close to the membrane interface
136 and a strongly electronegative 'cap' that sits at the cytoplasmic end of the structure (Fig. 2c, d, e). For the
137 basic belt, each monomer contributes six lysine residues at positions 44, 52, 56, 81, 108, and 206 and
138 twelve arginine residues at positions 53, 54, 57, 66, 110, 114, 117, 118, 124, 128, 200, and 222. For the
139 cap, each monomer contributes seven aspartates at positions 73, 77, 102, 103, 211, 223, and 225, and
140 eleven glutamate residues at positions 47, 58, 64, 90, 94, 96, 99, 105, 109, 116, and 227. Residues E105
141 and E109 line the cytoplasmic pore where we observed a single calcium ion in our structure (Fig. 2c, d).

The electrostatic properties of the inside of the ExbB pentamer mirror those on the outside where the large cavity is strongly electropositive, shifting to strongly electronegative near the cytoplasmic cap (Fig. 2f).

ExbB is a pentamer within the Ton complex

To further validate the pentameric state of ExbB observed in the X-ray crystal structure, negative stain electron microscopy (EM) was performed on two-dimensional (2D) crystals of the full-length ExbB/ExbD complex (Fig. 3a). The 2D crystals were only poorly ordered as inspection of the power spectra of recorded images shows mostly diffuse spots that are visible up to about 30 Å. However, the best images were used to generate an averaged 2D projection map of the unit cell which revealed five subunits arranged as a pentamer with a centralized pore. Each of the globular domains has a diameter of 20-25 Å with the edges of the pentamer measuring ~45 Å, agreeing well with the crystal structure (Fig. 3b). The averaged maps show two different populations of the pentamer which are similar in size but differ in level intensity due to opposite orientations of the complex within the crystal; a similar packing arrangement was also observed in our crystal structures (Supplementary Fig. 8). ExbD was not detected in our EM studies, likely due to disorder of the globular domain which is anchored to the membrane by a long unstructured linker[15].

The Ton subcomplex was also studied in frozen solution using double electron-electron resonance (DEER) spectroscopy, where ExbB was labeled at C25 using the spin label MTSL. From this, distance distributions were obtained experimentally and compared to simulations of the *in silico* labeled crystal structure (Fig. 3c and Supplementary Fig. 9). The experimental results agree remarkably well with the simulated distances with peaks at ~35 and 50-60 Å (Fig. 3d). Together with the crystal structure and EM studies, these results further verify the stoichiometry of ExbB as a pentamer within the Ton subcomplex containing a centralized TM pore (Fig. 3b, d).

To determine the oligomeric state of ExbB in the presence of TonB, the fully assembled Ton complex was expressed and purified, and found to have a larger hydrodynamic radius than the ExbB/ExbD

subcomplex (Fig. 3e). Further, SDS-PAGE analysis showed no significant changes in the oligomeric ratio between ExbB and ExbD (Supplementary Fig. 10). We then labeled ExbB at position 25 with MTSL and repeated the DEER spectroscopy analysis, finding that the distance distributions were nearly identical to the subcomplex (Fig. 3f and Supplementary Fig. 9), confirming that ExbB is a pentamer both in the absence and presence of TonB.

ExbD is a dimer within the Ton complex

In our low pH crystal structures, we verified the presence of a single TMH from ExbD within the hydrophobic TM pore of ExbB. However, previous studies have suggested that the Ton complex may contain a dimer of ExbD[31]. To investigate this further, we engineered an $ExbB_{C25S}/ExbD_{E113C}$ construct of the Ton subcomplex which we used for crosslinking studies. The sample was incubated with the crosslinker $BM(PEG)_2$ and then separated by SEC and compared to a control sample that was not crosslinked (Fig. 4a). SDS-PAGE analysis confirmed the shift of ExbD from monomer to dimer for the crosslinked sample; however, no shift was observed by SEC, indicating that the ExbD-crosslinked dimer was being formed within a single complex (intra) rather than between two different complexes (inter).

To further explore the oligomeric state of ExbD within the Ton subcomplex, DEER spectroscopy was performed by labeling ExbD at residues 78 and 113 individually, and constructs of $ExbB_{C25S}/ExbD_{N78C}$ and $ExbB_{C25S}/ExbD_{E113C}$ were labeled with the spin label MTSL. Distance distributions were then detected experimentally and compared to simulations of an *in silico* labeled model of the ExbD dimer (PDB ID 2PFU)[15], which was based on the related TolR dimer structure (PDB ID 2JWK)[32] (Fig. 4b, c and Supplementary Fig. 9). The fact that distance measurements could be observed indicates that at least a dimer of ExbD is present in the subcomplex. Further, according to the dimer model, labeling at residue 78 would yield distances between 32 - 44 Å, which is consistent with the peaks observed experimentally at 35 and 43 Å (Fig. 4b, d). Furthermore, labeling at residue 113 would yield distances from 21 – 35 Å, which is

also consistent with the peaks observed experimentally at 23 and 34 Å, within the accuracy of the rotamer library approach (Fig. 4c, d and Supplementary Fig. 9).

To determine the oligomeric state of ExbD in the presence of TonB, DEER spectroscopy was performed on the fully assembled Ton complex containing the $TonB_{C18A}$, $ExbB_{C25S}$ and $ExbD_{N78C}$ mutations and labeled with MTSL. As was observed for ExbB, the distance distributions for the labels on ExbD were nearly identical to the subcomplex (Fig. 4e and Supplementary Fig. 9), confirming that ExbD is a dimer both in the absence and presence of TonB.

Channel properties of the Ton subcomplex

The Ton complex depends on the pmf for energy transduction and is rendered non-functional in the presence of the protonophore carbonylcyanide-m-chlorophenylhydrazone (CCCP), indicating that the Ton complex is driven by the pmf[27,33]. To investigate ion conduction by the Ton subcomplex (ExbB/ExbD), it was reconstituted into liposomes, which were fused with a preformed planar bilayer membrane as described previously[34]. Single and multi-channel recordings under symmetrical salt conditions (100 mM KCl) revealed that channels formed by the Ton subcomplex display a 120+/-30 pS conductance at neutral pH (Fig. 5a,b), whereas channels formed by the ExbB pentamer are nearly twice as large with a 220+/-50 pS conductance (Fig. 5b). This is consistent with our structure which shows the TM helix of ExbD plugging the TM pore of the ExbB pentamer.

Furthermore, ion selectivity of the channels was determined under non-symmetric salt conditions (100 and 400 mM KCl in *cis* and *trans* compartments, respectively). Channels of the Ton subcomplex have a pronounced cation selectivity with 7-fold larger permeability for K^+ compared with Cl^- (V_{rev}, +24.7 ± 0.9 mV; pK^+/pCl^-, 7.0 ± 0.9) (Supplementary Table 2). Channels formed by the $ExbB/ExbD_{\Delta peri}$ complex are less cation selective (V_{rev}, +13.7 ± 4.5 mV; pK^+/pCl^-, 2.6 ± 1.0), which implies that the periplasmic domain of ExbD enhances cation selectivity. However, the ExbB pentamer is anion-selective (V_{rev}, -12.6 ± 2.8 mV; pK^+/pCl^-, 0.43 ± 0.09) (Supplementary Table 2), indicating that $ExbD_{\Delta peri}$ is sufficient to serve as a cation

selective filter. The point mutation D25A, found within the TM helix of ExbD which sits in the pore of the ExbB pentamer, significantly decreases the cation selectivity of the Ton subcomplex (V_{rev}, +17.0 ± 1.5 mV; pK^+/pCl^-, 3.3 ± 0.5) (Supplementary Table 2), indicating a major contribution of D25 towards ion selectivity.

We also studied the pH dependence of the subcomplex by looking for changes in the transmembrane current. Channel activity of the Ton subcomplex has a pronounced pH dependence, showing a significant decrease in transmembrane current upon pH decrease from neutral to acidic (Fig. 5c). However, the TM helix of ExbD is not the major contributor to the observed pH dependence, as the D25A mutant shows nearly an identical pH dependence as observed for wild-type (Fig. 5c), suggesting that the unique electrostatic properties of the ExbB pentamer may be responsible. The decrease in transmembrane current amplitude in the pH range 4.5-8.0 is explained by a decrease in single channel conductance from 120 pS to 70 pS at pH 8.0 and 4.5, respectively (Fig. 5d). Below pH 4.5, the decrease in transmembrane current is caused by channel closure at both positive and negative potentials (Fig. 5c). The ion channel conductance properties of the Ton subcomplex demonstrate that it is being modulated by pH, possibly caused by movement of the TM helix of ExbD within the TM pore of the ExbB pentamer, such that at low pH, the TM helix of ExbD is in a more closed/fixed conformation (Fig. 2b). This hypothesis is in agreement with our crystallographic studies where we observed that the TM helix of ExbD was most ordered at low pH.

Model for the fully assembled Ton complex

Taken together, our crystallography, EM, DEER, and crosslinking studies suggest that the Ton subcomplex consists of a pentamer of ExbB and a dimer of ExbD, where one copy of ExbD sits within the TM pore of the ExbB pentamer; CD analysis showed that the presence of ExbD significantly stabilizes the subcomplex (Supplementary Fig. 11). And given the vast buried surface area of each monomer (~3,000 $Å^2$; ~20% of total surface area), it is unlikely that the ExbB pentamer dissociates within the membrane,

241 indicating that ExbB likely oligomerizes around the inside ExbD during biogenesis of the complex. Since
242 only a single TM helix can fit within the TM pore of ExbB, and dimerization of ExbD is hypothesized to be
243 mediated by its periplasmic domain, we suggest that a second copy of ExbD is located outside of the ExbB
244 pentamer. Previous studies have indicated that TonB may exchange for one of the ExbD monomers during
245 energy transduction[17]. However, our studies show that association of TonB does not significantly affect the
246 structure or stoichiometry of ExbB or ExbD within the Ton complex. Based on our work, we propose a
247 model where the Ton complex consists of a pentamer of ExbB, a dimer of ExbD, and at least one TonB
248 (Fig. 5e). The interaction of TonB with ExbD represents the functional Ton complex, triggering energy
249 production and transduction in the form of conformational changes in TonB that leads to ligand uptake by
250 the transporter at the OM[35,36].

251 The Ton complex relies on the pmf for its function[27,33]; however, exactly how it is harnessed for
252 active transport is unclear. It has been proposed that the Ton complex acts as a proton-conducting channel
253 that shuttles protons from the periplasm to the cytoplasm and this powers a mechanical motion within the
254 complex[20]. Mutagenesis studies have previously identified a number of residues that are necessary for
255 harnessing the pmf, including D25 of ExbD and T148 and T181 of ExbB[37,38]. These residues all map to the
256 interior of the TM pore of ExbB where protons would be translocated (Supplementary Fig. 12). Our
257 crystallographic studies indicate that the TM helix of ExbD is quite dynamic within the TM pore of ExbB,
258 and together with the electrophysiology experiments, show that this dynamic behavior can be modulated by
259 pH. The electrostatics of the ExbB pentamer may also create an 'electrostatic funneling' effect which
260 assists in drawing protons from the periplasm and steering them through the TM pore of ExbB into the
261 cytoplasm (Fig. 5f). Therefore, we suggest two plausible mechanistic models for how the Ton complex
262 harnesses the pmf for energy production and transduction (Fig. 5g). The first is the 'electrostatic piston'
263 model, where the TM helix of ExbD moves translationally within the TM pore of ExbB, thereby creating a
264 piston-like motion. And the second is the 'rotational' model, where the TM helix of ExbD rotates within
265 the TM pore of ExbB, creating rotational motion. A combination of the two mechanistic models is also

plausible. While we observe minor conformational shifts within the TM helices of ExbB in our structures, it is also feasible that the ExbB pentamer cycles through more pronounced conformations to either drive or accommodate the dynamics of the TM helix of ExbD.

Given the homology to both the Tol and Mot complexes, our work with the Ton complex will also drive further efforts to understand those systems to determine exactly how the components of the complexes work in concert to convert the pmf into mechanical energy used to power these molecular machines. It will also be important to determine the structure of the fully assembled Ton complex to define the interactions of the periplasmic domains of ExbD and TonB to decipher exactly how energy is generated and transduced to the OM.

Methods Summary

The Ton complex and subcomplexes were expressed by co-transformation into BL21(DE3) cells, solubilized directly from membranes, and purified using a 6x-His tag. Crystallization was performed by vapor diffusion, data collected at the GM/CA-CAT and SER-CAT beamlines at the Advanced Photon Source and processed with HKL2000[39] and Xia2[40], and the initial structure solved by Se-SAD using HKL2MAP[41] and PHENIX/AutoSol[42]; other structures were solved by molecular replacement using PHENIX/PHASER[42,43]. 2D crystals were grown by the dialysis method, EM images collected on a Tecnai G2 200 LaB6 electron microscope, and processed using ImageJ[44] and the IPLT Correlation Averaging suite[45]. For DEER analysis, samples were labeled with MTSL, analyzed using a Bruker ELEXSYS E580Q-AWG dedicated pulse Q-band spectrometer, and distance distributions calculated with DeerAnalysis2015 and simulated with MMM2015[46,47]. Crosslinking studies were performed by incubation with $BM(PEG)_2$ followed by analysis with SEC and SDS-PAGE. Channel measurements were performed in planar-lipid bilayers. For more details see Methods.

Supplementary Information is linked to the online version of the paper at www.Nature.com/nature.

Acknowledgements

We would like to thank the respective staffs at the Southeast Regional Collaborative Access Team (SER-CAT) and General Medicine and Cancer Institute's Collaborative Access Team (GM/CA-CAT) beamlines at the Advanced Photon Source, Argonne National Laboratory for their assistance during data collection. Use of the Advanced Photon Source was supported by the US Department of Energy, Office of Science, Office of Basic Energy Sciences, under Contract No. W-31-109-Eng-38 (SER-CAT), and by the US Department of Energy, Basic Energy Sciences, Office of Science, under contract No. DE-AC02-06CH11357 (GM/CA-CAT). In addition, we would like to thank the staffs at beamlines 5.0.1 and 8.2.1 of the Advance Light Source at Lawrence Berkeley National Laboratory for their assistance during crystal screening. The Advanced Light Source is supported by the Director, Office of Science, Office of Basic Energy Sciences, of the U.S. Department of Energy under Contract No. DE-AC02-05CH11231. We would like to thank G. Jeschke (ETH Zurich) for providing the Q-band resonator, T. Assafa for the reproducibility measurements, the Deutsche Forschungsgemeinschaft for funding the AWG E580 Q-band spectrometer (INST 130/972-1 FUGG), and Yan Li at the NINDS/NIH Protein/Peptide Sequencing Facility for performing mass spectrometry analysis. NN is supported by the Department of Biological Sciences at Purdue University and by the National Institute of Allergy and Infectious Diseases (1K22AI113078-01). WAC is supported by the National Institutes of Health (NIH GM 038323) and the Henry Koffler Professorship at Purdue University. RL is supported by grants from the Agence National de la Recherche (BACMOLMOT [ANR-14-CE09-0023]) and from Projets internationaux de coopération scientifique (PICS05853). HC, TB and SKB are supported by the Intramural Research Program of the National

Institutes of Health, National Institute of Diabetes and Digestive and Kidney Diseases. EB is supported by the Cluster of Excellence RESOLV (EXC 1069) funded by the Deutsche Forschungsgemeinschaft.

Author Contributions

MS prepared the ExbB wild-type construct. HC, NN, TB, and RL prepared ExbD constructs and mutants of ExbB and ExbD. TB prepared the TonB constructs. HC performed all expression and purification for assays, EM, DEER, electrophysiology, and crystallization. HC and NN performed crystallization and HC, NN, and IB did screening and data collection. NN solved the initial crystal structure using crystals grown by HC. HC performed the EM experiments. EB performed the DEER experiments. SZ and WC performed the electrophysiology experiments. All authors analyzed and discussed the data. RL, WC, and SKB conceived the original projects. HC, NN, SZ, WC, RL and SKB contributed to writing the manuscript.

Author Information

Coordinates and structure factors for the ExbB/ExbD complexes have been deposited into the Protein Data Bank (accession codes YYYY, and ZZZZ). The authors declare no competing financial interests.
Correspondence and requests for materials should be addressed to S.K.B. (skbuchan@helix.nih.gov), N.N. (nnoinaj@purdue.edu), or R.L. (lloubes@imm.cnrs.fr).

References

1 Krewulak, K. D. & Vogel, H. J. TonB or not TonB: is that the question? *Biochem. Cell Biol.* **89**, 87-97 (2011).

2 Noinaj, N., Guillier, M., Barnard, T. J. & Buchanan, S. K. TonB-dependent transporters: regulation, structure, and function. *Annu. Rev. Microbiol.* **64**, 43-60 (2010).

3 Bassford, P. J., Jr., Bradbeer, C., Kadner, R. J. & Schnaitman, C. A. Transport of vitamin B12 in tonB mutants of Escherichia coli. *J. Bacteriol.* **128**, 242-247 (1976).

4 Lohmiller, S., Hantke, K., Patzer, S. I. & Braun, V. TonB-dependent maltose transport by Caulobacter crescentus. *Microbiology* **154**, 1748-1754 (2008).

5 Schauer, K., Rodionov, D. A. & de Reuse, H. New substrates for TonB-dependent transport: do we only see the 'tip of the iceberg'? *Trends Biochem. Sci.* **33**, 330-338 (2008).

6 Cascales, E. *et al.* Colicin biology. *Microbiol. Mol. Biol. Rev.* **71**, 158-229 (2007).

7 Postle, K. & Kadner, R. J. Touch and go: tying TonB to transport. *Mol. Microbiol.* **49**, 869-882 (2003).

8 Clement, E., Mesini, P. J., Pattus, F. & Schalk, I. J. The binding mechanism of pyoverdin with the outer membrane receptor FpvA in Pseudomonas aeruginosa is dependent on its iron-loaded status. *Biochemistry* **43**, 7954-7965 (2004).

9 Cadieux, N., Barekzi, N. & Bradbeer, C. Observations on the calcium dependence and reversibility of cobalamin transport across the outer membrane of Escherichia coli. *J. Biol. Chem.* **282**, 34921-34928 (2007).

10 Schramm, E., Mende, J., Braun, V. & Kamp, R. M. Nucleotide sequence of the colicin B activity gene cba: consensus pentapeptide among TonB-dependent colicins and receptors. *J. Bacteriol.* **169**, 3350-3357 (1987).

11 Brewer, S. *et al.* Structure and function of X-Pro dipeptide repeats in the TonB proteins of Salmonella typhimurium and Escherichia coli. *J. Mol. Biol.* **216**, 883-895 (1990).

12 Chang, C., Mooser, A., Pluckthun, A. & Wlodawer, A. Crystal structure of the dimeric C-terminal domain of TonB reveals a novel fold. *J. Biol. Chem.* **276**, 27535-27540 (2001).

13 Witty, M. *et al.* Structure of the periplasmic domain of Pseudomonas aeruginosa TolA: evidence for an evolutionary relationship with the TonB transporter protein. *EMBO J.* **21**, 4207-4218 (2002).

14 Kodding, J. *et al.* Crystal structure of a 92-residue C-terminal fragment of TonB from Escherichia coli reveals significant conformational changes compared to structures of smaller TonB fragments. *J. Biol. Chem.* **280**, 3022-3028 (2005).

15 Garcia-Herrero, A., Peacock, R. S., Howard, S. P. & Vogel, H. J. The solution structure of the periplasmic domain of the TonB system ExbD protein reveals an unexpected structural homology with siderophore-binding proteins. *Mol. Microbiol.* **66**, 872-889 (2007).

16 Higgs, P. I. *et al.* Quantification of known components of the Escherichia coli TonB energy transduction system: TonB, ExbB, ExbD and FepA. *Mol. Microbiol.* **44**, 271-281 (2002).

17 Sverzhinsky, A. *et al.* Membrane Protein Complex ExbB4-ExbD1-TonB1 from Escherichia coli Demonstrates Conformational Plasticity. *J. Bacteriol.* **197**, 1873-1885 (2015).

18 Sverzhinsky, A. *et al.* Coordinated rearrangements between cytoplasmic and periplasmic domains of the membrane protein complex ExbB-ExbD of Escherichia coli. *Structure* **22**, 791-797 (2014).

19 Pramanik, A. *et al.* Oligomeric structure of ExbB and ExbB-ExbD isolated from Escherichia coli as revealed by LILBID mass spectrometry. *Biochemistry* **50**, 8950-8956 (2011).

20 Jordan, L. D. *et al.* Energy-dependent motion of TonB in the Gram-negative bacterial inner membrane. *Proc. Natl. Acad. Sci. U. S. A.* **110**, 11553-11558 (2013).

21 Braun, V. The structurally related exbB and tolQ genes are interchangeable in conferring tonB-dependent colicin, bacteriophage, and albomycin sensitivity. *J. Bacteriol.* **171**, 6387-6390 (1989).

22 Cascales, E., Lloubes, R. & Sturgis, J. N. The TolQ-TolR proteins energize TolA and share homologies with the flagellar motor proteins MotA-MotB. *Mol. Microbiol.* **42**, 795-807 (2001).

23 Lloubes, R. *et al.* The Tol-Pal proteins of the Escherichia coli cell envelope: an energized system required for outer membrane integrity? *Res. Microbiol.* **152**, 523-529 (2001).

24 Yeh, Y. C., Comolli, L. R., Downing, K. H., Shapiro, L. & McAdams, H. H. The caulobacter Tol-Pal complex is essential for outer membrane integrity and the positioning of a polar localization factor. *J. Bacteriol.* **192**, 4847-4858 (2010).

25 Gray, A. N. *et al.* Coordination of peptidoglycan synthesis and outer membrane constriction during Escherichia coli cell division. *Elife* **4** (2015).

26 Germon, P., Ray, M. C., Vianney, A. & Lazzaroni, J. C. Energy-dependent conformational change in the TolA protein of Escherichia coli involves its N-terminal domain, TolQ, and TolR. *J. Bacteriol.* **183**, 4110-4114 (2001).

27 Larsen, R. A., Thomas, M. G. & Postle, K. Protonmotive force, ExbB and ligand-bound FepA drive conformational changes in TonB. *Mol. Microbiol.* **31**, 1809-1824 (1999).

28 Zhai, Y. F., Heijne, W. & Saier, M. H., Jr. Molecular modeling of the bacterial outer membrane receptor energizer, ExbBD/TonB, based on homology with the flagellar motor, MotAB. *Biochim. Biophys. Acta* **1614**, 201-210 (2003).

29 Kojima, S. & Blair, D. F. Conformational change in the stator of the bacterial flagellar motor. *Biochemistry* **40**, 13041-13050 (2001).

30 Saier, M. H., Jr. Tracing pathways of transport protein evolution. *Mol. Microbiol.* **48**, 1145-1156 (2003).

31 Ollis, A. A., Manning, M., Held, K. G. & Postle, K. Cytoplasmic membrane protonmotive force energizes periplasmic interactions between ExbD and TonB. *Mol. Microbiol.* **73**, 466-481 (2009).

32 Parsons, L. M., Grishaev, A. & Bax, A. The periplasmic domain of TolR from Haemophilus influenzae forms a dimer with a large hydrophobic groove: NMR solution structure and comparison to SAXS data. *Biochemistry* **47**, 3131-3142 (2008).

33 Larsen, R. A. & Postle, K. Conserved residues Ser(16) and His(20) and their relative positioning are essential for TonB activity, cross-linking of TonB with ExbB, and the ability of TonB to respond to proton motive force. *J. Biol. Chem.* **276**, 8111-8117 (2001).

34 Labarca, P. & Latorre, R. Insertion of ion channels into planar lipid bilayers by vesicle fusion. *Methods Enzymol.* **207**, 447-463 (1992).

35 Ollis, A. A., Kumar, A. & Postle, K. The ExbD periplasmic domain contains distinct functional regions for two stages in TonB energization. *J. Bacteriol.* **194**, 3069-3077 (2012).

36 Ollis, A. A. & Postle, K. ExbD mutants define initial stages in TonB energization. *J. Mol. Biol.* **415**, 237-247 (2012).

37 Braun, V. *et al.* Energy-coupled transport across the outer membrane of Escherichia coli: ExbB binds ExbD and TonB in vitro, and leucine 132 in the periplasmic region and aspartate 25 in the transmembrane region are important for ExbD activity. *J. Bacteriol.* **178**, 2836-2845 (1996).

38 Braun, V. & Herrmann, C. Point mutations in transmembrane helices 2 and 3 of ExbB and TolQ affect their activities in Escherichia coli K-12. *J. Bacteriol.* **186**, 4402-4406 (2004).

39 Minor, Z. O. a. W. Processing of X-ray Diffraction Data Collected in Oscillation Mode. *Methods Enzymol.* **276**, 307-326 (1997).

40 Winter, G. xia2: an expert system for macromolecular crystallography data reduction. *J. Appl. Cryst* **43**, 186-190 (2010).

41 Schneider, T. P. T. R. HKL2MAP: a graphical user interface for phasing with SHELX programs. *J. Appl. Cryst* **37**, 843-844 (2004).

42 Adams, P. D. *et al.* PHENIX: a comprehensive Python-based system for macromolecular structure solution. *Acta Crystallogr. D Biol. Crystallogr.* **66**, 213-221 (2010).

43 McCoy, A. J. *et al.* Phaser crystallographic software. *J Appl Crystallogr* **40**, 658-674 (2007).

44 Schneider, C. A., Rasband, W. S. & Eliceiri, K. W. NIH Image to ImageJ: 25 years of image analysis. *Nat Methods* **9**, 671-675 (2012).

45 Schenk, A. D., Philippsen, A., Engel, A. & Walz, T. A pipeline for comprehensive and automated processing of electron diffraction data in IPLT. *J. Struct. Biol.* **182**, 173-185 (2013).

46 Jeschke, G., Chechik, V., Ionita, P., Godt, A., Zimmermann, H., Banham, J., Timmel, C.R., Hilger, D., and Jung, H. . DeerAnalysis2006—a comprehensive software package for analyzing pulsed ELDOR data. *Appl. Magn. Reson.* **30** (2006).

47 Polyhach, Y., Bordignon, E. & Jeschke, G. Rotamer libraries of spin labelled cysteines for protein studies. *Phys. Chem. Chem. Phys.* **13**, 2356-2366 (2011).

48 Sehnal, D. *et al.* MOLE 2.0: advanced approach for analysis of biomacromolecular channels. *J. Cheminform.* **5**, 39 (2013).

49 Smart, O. S., Neduvelil, J. G., Wang, X., Wallace, B. A. & Sansom, M. S. HOLE: a program for the analysis of the pore dimensions of ion channel structural models. *J. Mol. Graph.* **14**, 354-360, 376 (1996).

Figure Legends

Figure 1. The structure of the ExbB oligomer. a. Schematic of the Ton system for energy transduction from the inner membrane (IM) to the outer membrane (OM). In response to pmf, the Ton complex, consisting of ExbB, ExbD, and TonB, transduces a mechanical energy to the OM via the C-terminal domain of TonB which directly interacts with transporters to allow ligand transport. **b.** Size-exclusion chromatography profile of the Ton subcomplexes (1, ExbB/ExbD; 2, ExbB/ExbD$_{\Delta peri}$) used for X-ray crystallography, EM, and electrophysiology experiments. **c.** SDS-PAGE analysis of the Ton subcomplexes purified in panel **b**. **d.** A cartoon representation of the ExbB monomer, consisting of seven α-helices. **e.** The ExbB pentamer structure shown as cartoon and transparent surface. The pentamer measures ~110 Å in height with ~60 Å extending into the cytoplasm. **f.** Perpendicular view of the cytoplasmic end of the ExbB pentamer depicting the 5-fold symmetry with each edge measuring ~45 Å. **g.** Perpendicular view of the periplasmic end of the ExbB pentamer illustrating the pseudo 5-fold symmetry with each edge measuring ~35 Å. **h.** The ExbB pentamer was analyzed with the programs MOLE 2.0[48] (spheres representation) and HOLE[49] (purple dots), highlighting the size of the large cavities. The pore radius was also analyzed for the entire length of the structure. **i.** A perpendicular view of the cavities in panel **h** to better illustrate the five fenestrations (vents) which could allow passage of solvent and ions.

Figure 2. The structure of the ExbB/ExbD$_{\Delta peri}$ complex. a. The ExbB/ExbD$_{\Delta peri}$ complex highlighting the TM helix of ExbD (blue) located within the TM pore of the ExbB pentamer (gray), which is offset by ~10 Å (blue dashed lines) from the membrane relative to the predicted TM domains of ExbB. Top panel shows the membrane (side) view, while the bottom panel shows a periplasmic view, illustrating the location of the ExbD TM helix within the TM pore of ExbB formed by helices α6 and α7. **b.** Residues from helices α6 and α7 line the TM pore of ExbB (gray) and mediate interaction with the TM helix of ExbD (blue). For clarity, only two monomers of the ExbB pentamer are shown. Of special interest are the locations of the conserved residues T148 and T181 of ExbB, which may play a role in proton transfer through the TM pore

and are found close to D25 of ExbD. **c.** The cytoplasmic domain of ExbB forms a large enclosed cavity that includes twelve arginines, six lysines, eleven glutamates, and seven aspartates from each monomer. The top panel shows the assembly of the ExbB pentamer highlighting the charged residues in the cytoplasmic domain, while the bottom panel shows the perpendicular view from the cytoplasmic end. **d.** Zoomed view of the electronegatively charged residues E105 and E109 lining the cytoplasmic pore and interacting with a single calcium ion (green sphere). **e.** Electrostatic surface representation of ExbB showing the electropositive 'belt', formed by the numerous arginine and lysine residues, and the electronegative 'cap', formed by the aspartate and glutamate residues. **f.** Cutaway view showing that the electrostatic surface properties of the inside cavity mimic those observed along the outside.

Figure 3. The oligomeric state of ExbB within the Ton complex. a. Electron microscopy (EM) analysis was performed using 2D crystals *(i)* of the Ton subcomplex with a power spectrum out to ~30 Å *(ii)* and an average projection map shows the complex is pentameric *(iii)*. Two pentamers are highlighted with yellow pentagons, with the difference in intensity due to staining of molecules in opposite orientations. **b.** The EM studies agree with the crystal structure showing that ExbB is a pentamer with edges measuring ~45 Å. **c.** DEER spectroscopy was performed on the Ton subcomplex labeled with MTSL at position C25 of ExbB. The experimentally measured traces (normalized primary data V(t)) and distance distributions (*inset*) (red lines) agree well with those calculated from the *in silico* labeled ExbB (black dashed lines). **d.** DEER analyses of the Ton subcomplex agree with the crystal structure showing that ExbB is a pentamer with spin label distances measuring ~35 Å (edges) and 50-60 Å (cross-diagonal). **e.** Purification of the fully assembled Ton complex (orange), which elutes earlier than the Ton subcomplex lacking TonB (blue); and verification by SDS-PAGE analysis. **f.** DEER spectroscopy was performed in DDM on the fully assembled Ton complex labeled at position 25 on ExbB. Comparison of distance distributions of the fully assembled Ton complex (solid orange line) to those of the Ton subcomplex in DDM lacking TonB (dashed red line) showed minimal differences, indicating the association of TonB does not affect the stoichiometry of ExbB within the Ton complex.

Figure 4. The oligomeric state of ExbD within the Ton complex. a. Crosslinking studies targeting ExbD are consistent with a dimer within the Ton subcomplex, as evidenced by an observed crosslinked dimer form via size-exclusion chromatography and SDS-PAGE following crosslinking (red, lane 2) compared to the non-crosslinked sample (blue, lane 1). **b.** DEER spectroscopy was performed on ExbD labeled at position 78 (purple lines) and position 113 (cyan lines) (panel **c**). The experimentally measured traces (normalized primary data V(t)) and distance distributions (*inset*) (purple and cyan lines) are consistent with those calculated (black dashed lines) from the *in silico* labeled ExbD dimer model (PDB ID 2PFU), which is based on the reported TolR structure (PDB ID 2JWK). **d.** The distance measurements within the *in silico* labeled ExbD dimer model are in agreement with those obtained experimentally at each site using DEER analysis, supporting the hypothesis that ExbD is a dimer within the Ton subcomplex. **e.** DEER spectroscopy was performed in DDM on the fully assembled Ton complex labeled at position 78 on ExbD. Using DEER spectroscopy, comparison of distance distributions of the fully assembled Ton complex (solid orange line) to those of the Ton subcomplex in DDM lacking TonB (dashed purple line) showed minimal differences, indicating the association of TonB does not affect the stoichiometry of ExbD within the Ton complex.

Figure 5. Channel properties of the Ton subcomplex. a. Representative spectra for single channel measurements of the Ton subcomplex (ExbB/ExbD) were performed in planar bilayers in symmetrical salt conditions (100 mM KCl solution, pH 7.5) at holding potentials of +50 (top) or -50 mV (bottom). **b.** Representative spectra of multichannel measurements performed on the Ton subcomplex (blue) and ExbB alone (green) at +/-50 mV. **c.** Dependence of the macroscopic current amplitude on the pH of the bathing solution for the Ton subcomplex (blue) and the D25A mutation in the TM helix of ExbD (green) with a holding potential of +50 mV (circles and squares) or -50 mV (triangles and diamonds). Data for macroscopic current were normalized. Significant channel closure was observed at pH ≤ 4.0. **d.** Dependence of single channel conductance of the Ton subcomplex on pH was measured at +50 mV. The largest channels (~120 pS) were observed at higher pH and size decreased as pH reached 4.4 (~70 pS) until

528 full closure at pH ~4.0 and below. **e**. Structural model for the Ton complex consisting of a pentamer of
529 ExbB, a dimer of ExbD, and at least one TonB. Together, the fully assembled Ton complex at the IM forms
530 a direct link for energy transduction to the transporters at the OM. **f**. The ExbB/ExbD$_{\Delta peri}$ complex showing
531 electric fields for the ExbB pentamer, which suggests that electrostatic funneling may assist in drawing
532 protons from the periplasm and steering them through the pore into the cytoplasm. The modeled location of
533 residue D25 of the TM helix of ExbD (purple helix) is indicated as a red sphere. **g**. Proposed mechanisms
534 for how the Ton subcomplex may use the pmf for the production of energy, which is then transduced to the
535 OM. With the 'electrostatic piston' model, the TM helix of ExbD moves translationally within the TM pore
536 of ExbB, thereby creating a piston-like motion. In the 'rotational' model, the TM helix of ExbD rotates
537 within the TM pore of ExbB.

538

Methods

Cloning of E. coli (K-12 strain) ExbB, ExbD, and TonB constructs and mutants.

The ExbB construct with and without a C-terminal 6x-His tag was subcloned into pET26b (Novagen). ExbD was subcloned into pACYCDuet-1 vector (Novagen) with an N-terminal Strep-tag and a C-terminal 6x-His tag. ExbD was also subcloned into pCDF-1b vector (Novagen) containing a C-terminal TEV protease site followed by a 6x-His tag. An $ExbD_{\Delta peri}$ construct containing a C-terminal TEV protease site [*preceded by a Gly-Gly-Gly linker for efficient digestion by TEV protease*] followed by a 6x-His tag was constructed by deletion of the sequence encoding the periplasmic domain of ExbD (residues 50 – 141). TonB was cloned into pACYCDUET-1 vector with an N-terminal 10x-His tag followed by a TEV protease site. Mutants of TonB (C18A), ExbD (D25A, N78C and E113C), and ExbB (C25S) were prepared by site-directed mutagenesis (primer sequences for all cloning and mutagenesis experiments are available upon request). The sequences of all plasmid constructs and mutations were verified by sequence analysis (Macrogen USA and Eurofins Genomics GmbH).

Expression and purification of the Ton complex, subcomplexes, and components.

Expression of ExbB with a C-terminal 6x-His tag was performed by transforming BL21(DE3) cells (NEB) with the pET26b/ExbB vector. Co-expression was performed by co-transforming BL21(DE3) cells with the respective ExbB, ExbD, and/or TonB plasmids. For all transformations, cells were plated onto LB agar plates supplemented with appropriate antibiotics. Colonies were then used for a starter culture to inoculate twelve flasks containing either 1 L of 2xYT medium (Ton subcomplex) or SelenoMet Media supplemented with L-methionine at 40 mg/L (Molecular Dimensions) (Ton complex), with appropriate antibiotics. Cultures were grown at 37°C with shaking at 220 rpm until OD_{600} of 0.5 – 1.0, induced with isopropyl β-D-1-thiogalactopyranoside (IPTG) to 0.1 mM final concentration, and then allowed to continue to grow overnight at 28°C. For selenomethionine-substituted samples for experimental phasing, B834(DE3) cells (NEB) were co-transformed with pET26b/$ExbB_{C25S}$ and pCDF-1b/$ExbD_{\Delta peri}$ plasmids. Single colonies

563 were used to inoculate twelve flasks containing 1 L SelenoMet Medium (Molecular Dimensions)
564 supplemented with 40 mg/mL selenomethionine and appropriate antibiotics. Cultures were grown at 37°C
565 with shaking at 220 rpm until OD_{600} of 0.5 – 1.0, induced with IPTG to 0.1 mM final concentration, and
566 then allowed to continue to grow overnight at 28°C. Cells were harvested and used immediately or stored at
567 -80°C.

568 For purification, cells were resuspended in either 1x PBS (Ton subcomplex) or TBS (Ton complex)
569 supplemented with 100 μM 4-(2-aminoethyl)benzenesulfonyl fluoride (AEBSF), 100 μM DNAse, and 50
570 μg/ml lysozyme, and disrupted with two passages through an EmulsiFlex-C3 (Avestin) operating at
571 ~15,000 psi. Membranes were pelleted by ultracentrifugation in a Type 45 Ti Beckman rotor at 200,000 x g
572 for 1 hr at 4°C. Membranes were then resuspended in 1x PBS or TBS using a dounce homogenizer and
573 solubilized by the addition of Triton X-100 (Ton subcomplex) or DDM (Anatrace) (Ton complex) to a final
574 concentration of 1% by stirring at medium speed for 1 hr to overnight at 4°C. Insoluble material was
575 pelleted by ultracentrifugation in a Type 45 Ti Beckman rotor at 200,000 x g for 1 hr at 4°C and the
576 supernatant was used immediately.

577 Immobilized metal affinity chromatography (IMAC) was performed on an AkTA Purifier (GE
578 Healthcare) using a 15 mL Ni-NTA agarose column (Qiagen) equilibrated with 1x PBS or TBS
579 supplemented with 0.1% Triton X-100 or 0.1% DDM. The supernatant was supplemented with 10 mM
580 imidazole and loaded onto the column. The column was washed in three steps with 1x PBS or TBS
581 supplemented with 20, 40 and 60 mM imidazole, respectively, and eluted with 1x PBS or TBS
582 supplemented with 250 mM imidazole in 2 mL fractions. Fractions were analyzed by SDS-PAGE and those
583 fractions containing the complex were pooled. To remove the 6x-His tag, TEV protease was added to the
584 sample at 0.1 mg/mL final concentration and rocked overnight at 4°C. For the Ton complex, the sample
585 was then diluted 2-3 times with 25 mM HEPES, pH 7.3, and 0.1% DDM and loaded onto an anion
586 exchange 6 ml ResourceQ column (GE Healthcare). Elution was performed with a 0-1 M NaCl gradient

over 5 column volumes. For the Ton subcomplex, the sample was concentrated using an Amicon Ultra-15 Centrifugal Filter Unit with a 50 kDa MW cut-off (Millipore), filtered, and purified by size-exclusion chromatography using a Superdex 200 HL 16/600 column (GE Healthcare) at a flow rate of 0.5-1.0 mL/min. The buffer consisted of 20 mM HEPES-NaOH, pH 7.0, 150 mM NaCl, 0.01% NaN_3, and 0.08% $C_{10}E_5$. For the Ton complex, eluted fractions were concentrated using an Amicon Ultra-15 Centrifugal Filter Unit with a 100 kDa MW cut-off (Millipore), and passed over a Superose6HR 10/30 column (GE Healthcare) at a flow rate of 0.5 mL/min using 20 mM HEPES-NaOH, pH 7.0, 150 mM NaCl, and 0.05% DDM.

Circular dichroism.

Far-UV circular dichroism (CD) spectra (185-260 nm) were measured in 0.1 M NaP_i, pH 7.0, and 0.03% DDM using quartz cuvettes with a 0.02 - 0.2 mm optical path length. The results were analyzed using the DichroWeb package of programs[50] and different sets of reference proteins, including the SMP180 set of membrane proteins. The analysis of the thermal stability of the complexes reconstituted into liposomes was measured by the temperature dependence of the CD signal amplitude at 222 nm. Thermal melting was performed in a magnetically stirred 1 cm quartz cuvette containing 10 mM HEPES, pH 7.0, and 100 mM NaCl with a rate of temperature increase of 0.5ºC/min. Melting curves were normalized to the measured value of the molar ellipticity change at 10ºC.

Crystallization and data collection.

For crystallization, samples were concentrated to ~10 mg/ml and sparse matrix screening was performed using a TTP Labtech Mosquito crystallization robot using hanging drop vapor diffusion and plates incubated at 15 - 21°C. Initially, many lead conditions were observed producing crystals with hexagonal morphology; however, none diffracted to better than ~7 Å and most suffered from anisotropy. To avoid this packing, we performed reductive methylation of our samples prior to crystallization using the Reductive Alkylation Kit (Hampton Research), followed by an additional size exclusion chromatography

step. This led to a condition which produced diffraction spots to ~4 Å resolution. Further optimization and screening allowed us to grow crystals in 100 mM Na-acetate, pH 4.5, 100 mM $MgCl_2$, and 25% PEG 400 that routinely diffracted ~3.5 Å resolution or better. For heavy atom soaking, crystals were transferred to a drop containing 1 mM $HgCl_2$ and incubated overnight at room temperature and then harvested directly from the soaking condition. The best native crystals for the ExbB/$ExbD_{\Delta peri}$ complex, however, were grown from 100 mM HEPES-NaOH, pH 7.0, 100 mM $CaCl_2$, and 22% PEG MME 550 and diffracted to 2.6 Å resolution; these crystals were also used for heavy atom soaking experiments. Unfortunately, none of the heavy atom soaked crystals (nor selenomethionine substituted crystals) were useful for phasing due to crystal pathologies which we suspected was twinning related. However, selenomethionine substituted crystals of the $ExbB_{C25S}$/$ExbD_{\Delta peri}$ complex were obtained using 100 mM MES/imidazole, pH 6.5, 30 mM $MgCl_2$, 30 mM $CaCl_2$, 50% ethylene glycol, and 8% PEG 8000 and diffracted to 5.2 Å resolution with no twinning related issues. Both native and selenomethionine-substituted crystals were harvested directly from the crystallization drops. Screening for diffraction quality was performed at the GM/CA-CAT and SER-CAT beamlines at the Advanced Photon Source at Argonne National Laboratory and at beamlines 5.0.1 and 8.2.1 at the Advanced Light Source at Lawrence Berkeley National Laboratory. Final datasets were collected at the SER-CAT beamline and all data were processed using either HKL2000[39] or Xia2[40]. A summary of the data collection statistics can be found in Supplementary Table 1. The presence of both components of the Ton subcomplex within the crystals was confirmed by SDS-PAGE and mass spectrometry analyses of harvested crystals.

Structure determination.

For phasing the ExbB/$ExbD_{\Delta peri}$ complex structure, three datasets were collected on selenomethionine substituted crystals of the $ExbB_{C25S}$/$ExbD_{\Delta peri}$ complex at a wavelength of 0.979 Å. The data were processed with Xia2[40] and based on non-isomorphism, one dataset was removed. The final two datasets were processed together in space group $P4_32_12$ to a final resolution of 5.2 Å. Selenium sites (35

total) were located using HKL2MAP[41] after 5000 tries within SHELXD at a resolution range of 20 – 6 Å. The sites were then fed into AutoSol (PHENIX)[42] which removed 1 site, producing a phase-extended density-modified electron density map which we could build an initial poly-alanine model into. Five-fold symmetry was clearly observed with each monomer consisting of very elongated α-helices and directionality was determined based on the predicted topology of ExbB, which contains a single large cytoplasmic domain. This model was then used as a search model to solve the native and Hg-soaked structures by molecular replacement using PHASER/PHENIX[42,43] and the sequence docked based on anomalous peaks from the SeSAD dataset. The ExbB/ExbD$_{\Delta peri}$ complex was solved in space group $P2_1$ to 2.6 Å resolution with R/Rfree values of 0.21/0.26 and the Hg-soaked structure in space group $P2_12_12_1$ to 3.5 Å resolution with R/Rfree values of 0.25/0.30. All model building was performed using COOT and subsequent refinement done in PHENIX[42]. RMSD analysis was performed within PyMOL (Schrödinger). Electrostatic surface properties (calculated using the Linearized Poisson-Boltzman Equation mode with a Solvent Radius of 1.4), including generation of the electric field lines, were analyzed and visualized using the APBS plugin within PyMOL (Schrödinger). Buried surface area was calculated using the PDBePISA server[51]. Structure-related figures were made with PyMOL (Schrödinger) and Chimera[52] and annotated and finalized with Adobe Photoshop and Illustrator.

Two-dimensional (2D) crystallization.

For two-dimensional (2D) crystallization experiments, the Ton subcomplex (ExbB/ExbD) was extracted and purified by IMAC as previously described. The sample was passed over a Superose 12 HR 10/30 column using 20 mM Tris-HCl, pH 7, 150 mM NaCl, 0.01% NaN_3, and 0.035% Triton X-100. The purified complex was then mixed with a solution stock of *E. coli* polar lipid (Avanti Polar Lipids, Inc) at 10 mg/ml in 2% Triton X-100, to reach final concentrations of 0.5-1.0 mg/mL protein and 0.1 to 0.4 mg/mL lipid. The lipid-protein-detergent samples solution were placed into Mini Slide-A-Lyser dialysis devices (Pierce) with a 20 kDa MW cutoff, and dialyzed in 1 L of 25 mM Tris-HCl, pH 7.0, 150 mM NaCl, and

0.01% NaN_3 at 4ºC. Aliquots of dialyzed samples were observed periodically by electron microscopy to monitor the formation of 2D crystals.

Electron microscopy.

Sample preparation for electron microscopy was carried out by applying a 5 µL drop of protein-lipid material on a glow discharged carbon-coated electron microscopy grid. Staining was performed by addition of 1% (w/v) uranyl acetate and incubation for 1 min. Grids were then imaged on a Tecnai G2 200 LaB6 electron microscope operating at 200 kV at the Institut de Microbiologie de la Méditerranée. Images were recorded with a 2K Eagle CCD camera.

The best 2D crystals were selected through observation of the power spectrum of the images using the ImageJ software[44]. Selected images were processed using the IPLT Correlation Averaging suite program[45]. A filtered image was generated by optical filtering of the low resolution spots, and padded to contain only 4-6 unit cells. The padded image was cross-correlated with the original large image. The positions of the cross-correlation peaks were determined and used to extract sub-images that were summed to generate an average image of the two-dimensional unit cell.

Double electron-electron resonance spectroscopy.

Site-directed spin labeling was used to covalently attach the spin label (1-Oxyl-2,2,5,5-tetramethyl-Δ3-pyrroline-3-methyl) methanethiosulfonate (MTSL) (Toronto Research Chemicals) to Cys25 on ExbB and to cysteines engineered at positions 78 and 113 on ExbD (N78C, E113C; ExbD constructs were in the pACYC vector containing an N-terminal strep-tag and a C-terminal 6x-HIS tag for the Ton subcomplex, and in the pCDF-1b vector for the Ton complex). For labeling with MTSL, samples were first incubated with 2-10 mM dithiothreitol (DTT) for 1-2 hr and the DTT then removed by passage over a HiTrap desalting column (GE Healthcare) or during anion exchange (Ton complex). Samples were then incubated with a 10x molar excess of MTSL overnight at 4ºC and then passed over a Superose 6HR 10/30 gel

682 filtration column (GE Healthcare) using 20 mM HEPES-NaOH, pH 7.5, 200 mM NaCl, 0.08% $C_{10}E_5$ or
683 0.03% DDM (Ton subcomplex); or 20 mM HEPES-NaOH, pH 7.0, 150 mM NaCl, and 0.05% DDM (Ton
684 complex).

685 For double electron-electron resonance (DEER) measurements, the samples were diluted with D_2O
686 to a final concentration of 30% and cryoprotected with 10% v/v D8-glycerol prior to being flash frozen in
687 liquid nitrogen. Continuous Wave (CW) EPR experiments were carried out at room temperature on a
688 bench-top X-band MiniScope MS 400 (Magnettech by Freiberg Instrument) at 9.5 GHz (X-band) with 2.5
689 mW microwave power, 15 mT sweep width, 0.15 mT modulation amplitude. Spin labeling efficiency was
690 calculated based on the second integral of the derivative spectra compared to a standard spin concentration
691 of 100 μM (Tempol in water). The ExbB native cysteine C25 was labeled with a 50% efficiency, while the
692 ExbD mutants were labeled with efficiencies > 80%. DEER measurements were initially performed at ETH
693 Zurich on a commercial Bruker ELEXSYS-II E580 Q-band spectrometer (34-35 GHz) and later on a
694 Bruker ELEXSYS E580Q-AWG dedicated pulse Q-band spectrometer operating at 34-35 GHz at FU
695 Berlin. Both spectrometers were equipped with a TWT amplifier (150 W) and a home-made rectangular
696 resonator (from ETH Zurich) enabling the insertion of 30-40 μL of sample volume in quartz tubes with 3
697 mm outer diameter[53]. Dipolar time evolution data were acquired using the four-pulse DEER experiment at
698 50 K. All pulses were set to be rectangular with 12 ns length, with the pump frequency at the maximum of
699 the echo-detected field swept spectrum, 100 MHz higher than the observer frequency. Deuterium nuclear
700 modulations were averaged by increasing the first interpulse delay by 16 ns for 8 steps as previously
701 described[53]. The background of the normalized DEER primary data (V(t)/V(0)) was fitted with optimized
702 dimensions from 2.5 to 3.2 and the resulting normalized secondary data (F(t)/F(0)) were converted by
703 model-free Tikhonov regularization to distance distributions with the software DeerAnalysis2015[46]. The
704 simulation of the possible spin label rotamers populated at selected positions in the protein was performed
705 using the Matlab program package MMM2015.1 using the MTSL ambient temperature library[47].

Crosslinking.

The $ExbB_{C25S}/ExbD_{E113C}$ complex ($ExbD_{E113C}$ was in the pACYC vector containing an N-terminal strep-tag and a C-terminal 6x-HIS tag) was expressed and purified as described earlier. To prepare the sample for crosslinking, the sample was incubated at 4°C with 5 mM DTT for at least 1 hr. The DTT was then removed using a desalting column in 20 mM HEPES, pH 7.0, 150 mM NaCl, and 0.1% DDM. The crosslinker 1,8-bismaleimidodiethylenglycol ($BM(PEG)_2$) (Pierce) was added at a final concentration of 0.2 mM and the reaction was incubated at 4°C overnight. The sample was concentrated and passed over a Superose 6HR 10/30 gel filtration column using 20 mM HEPES-NaOH, pH 7.0, 150 mM NaCl, and 0.035% DDM on an AkTA Purifier system (GE Healthcare). The results were visualized by SDS-PAGE analysis.

Reconstitution in liposomes.

Protein complexes were reconstituted into liposomes by dialysis of the protein/lipid/detergent mixture. Lipids (DOPG, DOPC and DOPE) dissolved in chloroform were mixed in a molar ratio 2:3:5. Chloroform was removed by vortexing in a stream of nitrogen gas in a glass tube followed by drying in vacuum for 2-3 hr. The lipid film was hydrated in 1 ml TN buffer (10 mM Tris-HCl, pH 7.5, 50 mM NaCl), followed by 5 cycles of freeze-thaw and sonication using a water bath sonicator until the suspension of lipids became clear (10-15 min). For proteoliposome preparation, small unilamellar vesicles (SUVs) were mixed with octylglucoside (final concentration, 2%) and then proteins added to achieve a molar ratio of total lipid to protein ≈500-2000 mol/mol. After 1 hr incubation in ice, the lipid/protein/detergent mixture was dialyzed into 10 mM Tris-HCl, pH 7.5, 0.3 M sucrose, and 50 mM KCl for 30-40 hr using a dialysis membrane with a MW cut-off pore size of 10 kDa.

Planar-lipid bilayer measurement of ion-conduction.

728 Mueller-Rudin type planar bilayer membranes were formed on a 0.2 mm diameter aperture in a
729 partition that separates two 1 mL compartments, using a mixture of lipids, DOPG, DOPC and DOPE, at a
730 molar ratio 2:3:5 (10 mg/mL) in n-decane, applied by a brush technique[54]. The aqueous solution in both
731 compartments consisted of 2 mM KP_i, pH 7.0, and 0.1 M and 0.4 M KCl in cis- and trans-compartments,
732 respectively. To study the pH dependence of channel activity, bathing solutions were buffered with 2 mM
733 Na-acetate (pK 4.8), Na-cacodylate (pK 6.2), and Tris (pK 8.3). The pH of the bathing solution was
734 changed by adding 10 - 20 μL 0.1 M HCl or KOH. The cis-side of the planar bilayer is defined as that to
735 which the electrical potential is applied. Proteoliposomes, 0.1-2 μL, were added to the trans-compartment,
736 and the solutions were stirred until the transmembrane current appeared. A large concentration of an
737 osmolyte inside of the liposomes and the transmembrane KCl concentration gradient caused
738 proteoliposome fusion with the pre-formed planar lipid membrane bilayer. The transmembrane current was
739 measured in voltage-clamp mode with Ag/AgCl electrodes and agar bridges, using a BC-525C amplifier
740 (Warner Instruments, Hamden, CT). Single channel conductance of the ExbB/ExbD complexes was
741 performed in symmetrical salt conditions: 0.1 M KCl solution, pH 7.5, at a holding potential of +50 or -50
742 mV.

743

744

745

746

747

748

749

750

References

50 Whitmore, L. & Wallace, B. A. Protein secondary structure analyses from circular dichroism spectroscopy: methods and reference databases. *Biopolymers* **89**, 392-400 (2008).

51 Krissinel, E. & Henrick, K. Inference of macromolecular assemblies from crystalline state. *J. Mol. Biol.* **372**, 774-797 (2007).

52 Pettersen, E. F. *et al.* UCSF Chimera--a visualization system for exploratory research and analysis. *J. Comput. Chem.* **25**, 1605-1612 (2004).

53 Polyhach, Y. *et al.* High sensitivity and versatility of the DEER experiment on nitroxide radical pairs at Q-band frequencies. *Phys. Chem. Chem. Phys.* **14**, 10762-10773 (2012).

54 Mueller, P., Rudin, D. O., Tien, H. T. & Wescott, W. C. Reconstitution of cell membrane structure in vitro and its transformation into an excitable system. *Nature* **194**, 979-980 (1962).

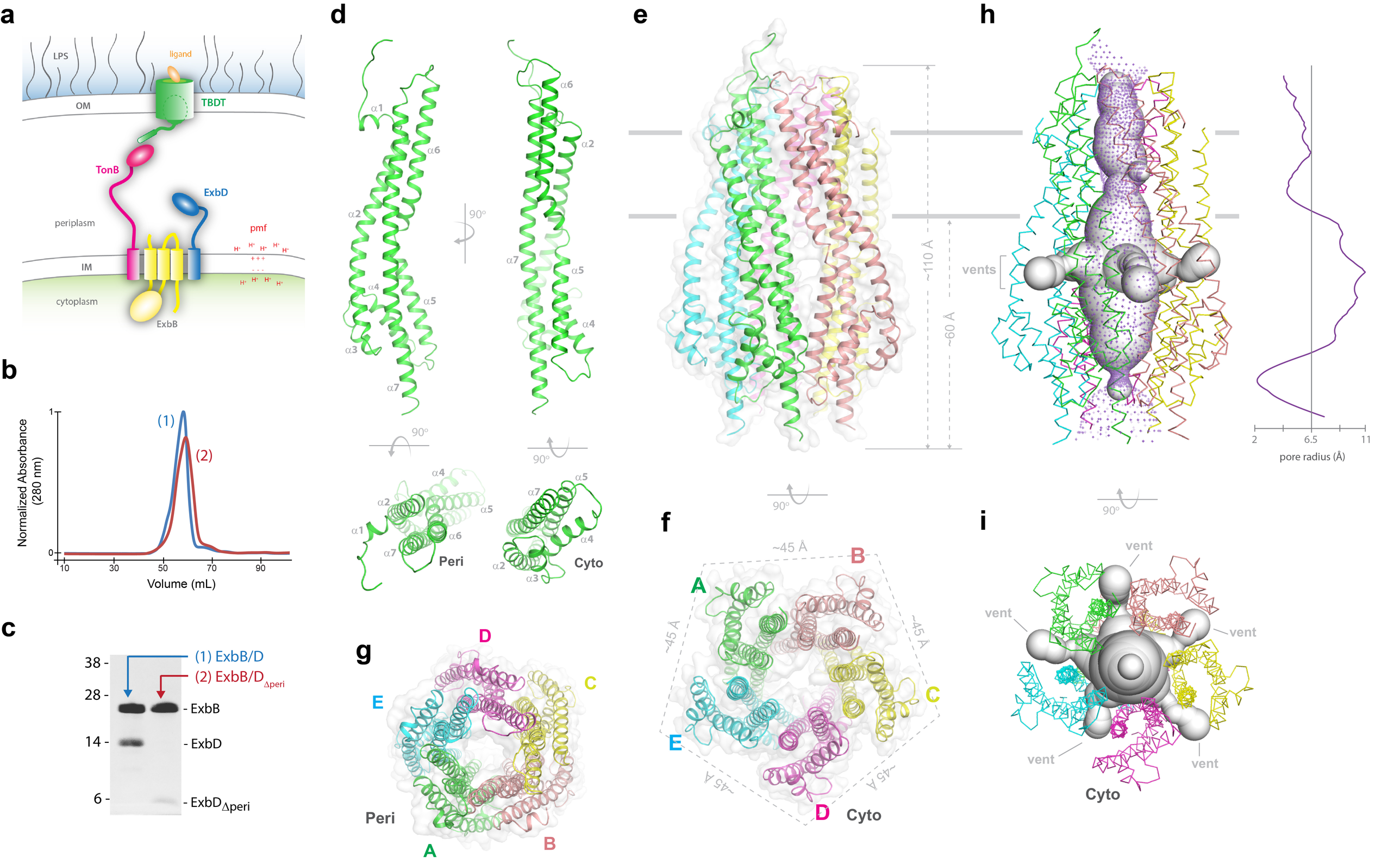
a
LPS
ligand
OM
TBDT
TonB
ExbD
periplasm
pmf
IM
cytoplasm
ExbB
b
Normalized Absorbance (280 nm)
Volume (mL)
(1)
(2)
c
(1) ExbB/D
(2) ExbB/D$_{\Delta peri}$
38 -
28 -
14 -
6 -
- ExbB
- ExbD
- ExbD$_{\Delta peri}$
d
α1
α2
α3
α4
α5
α6
α7
90°
Peri
Cyto
e
~110 Å
~60 Å
f
~45 Å
A
B
C
D
E
g
Peri
Cyto
h
vents
pore radius (Å)
2
6.5
11
i
vent
Cyto

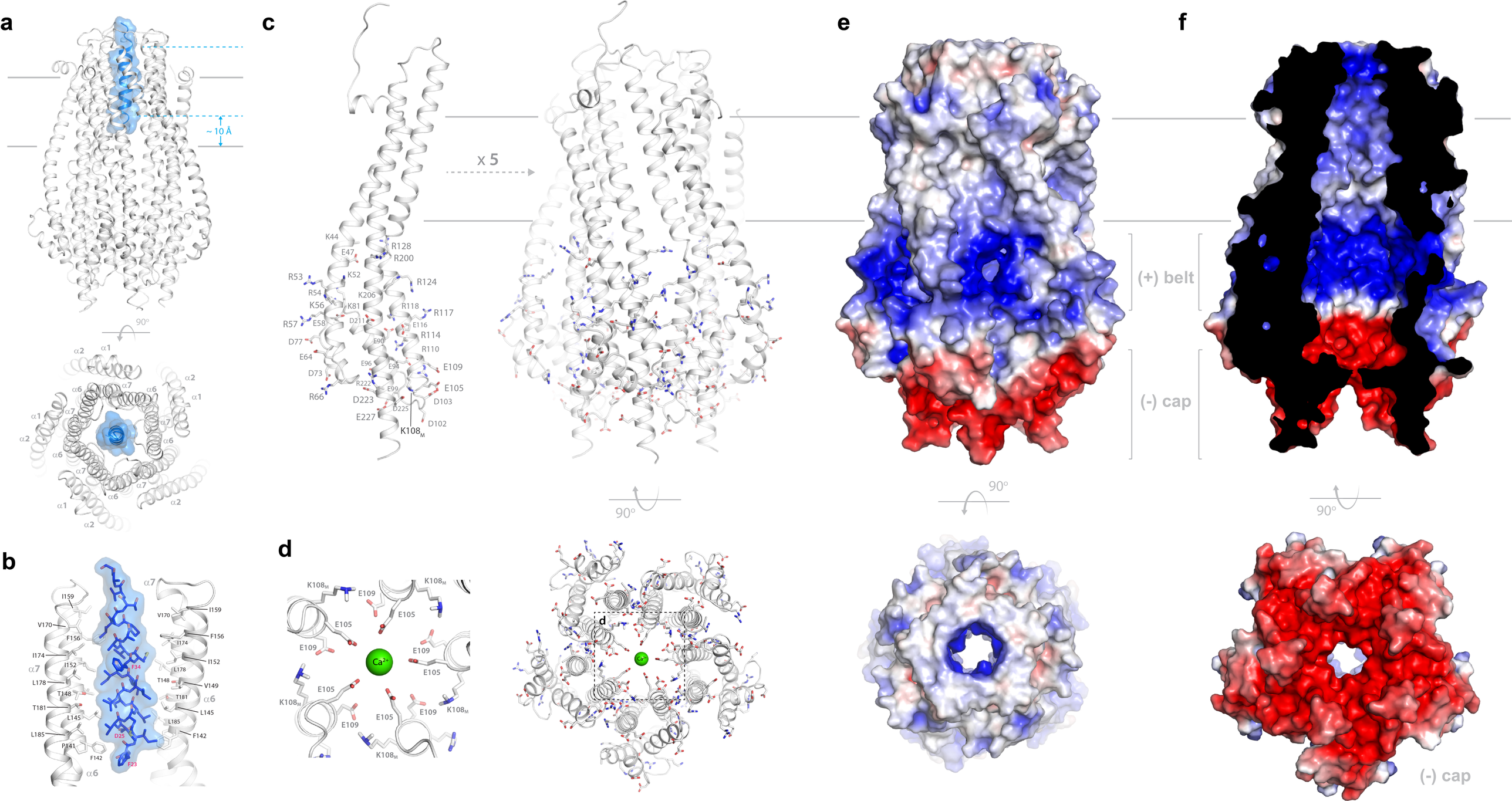
a
~ 10 Å
90°
α1
α2
α6
α7
b
I159
V170
F156
I174
I152
α7
L178
T148
T181
L145
L185
P141
F142
α6
F34
D25
F23
V149
α6
c
x 5
K44
E47
R128
R200
R53
K52
R124
R54
K206
K56
K81
R118
R117
R57
E58
D211
E116
D77
E90
R114
E64
R110
E96
E94
E109
D73
R222
E99
E105
R66
D223
D225
D103
E227
D102
K108M
d
Ca2+
e
(+) belt
(-) cap
90°
f
(-) cap

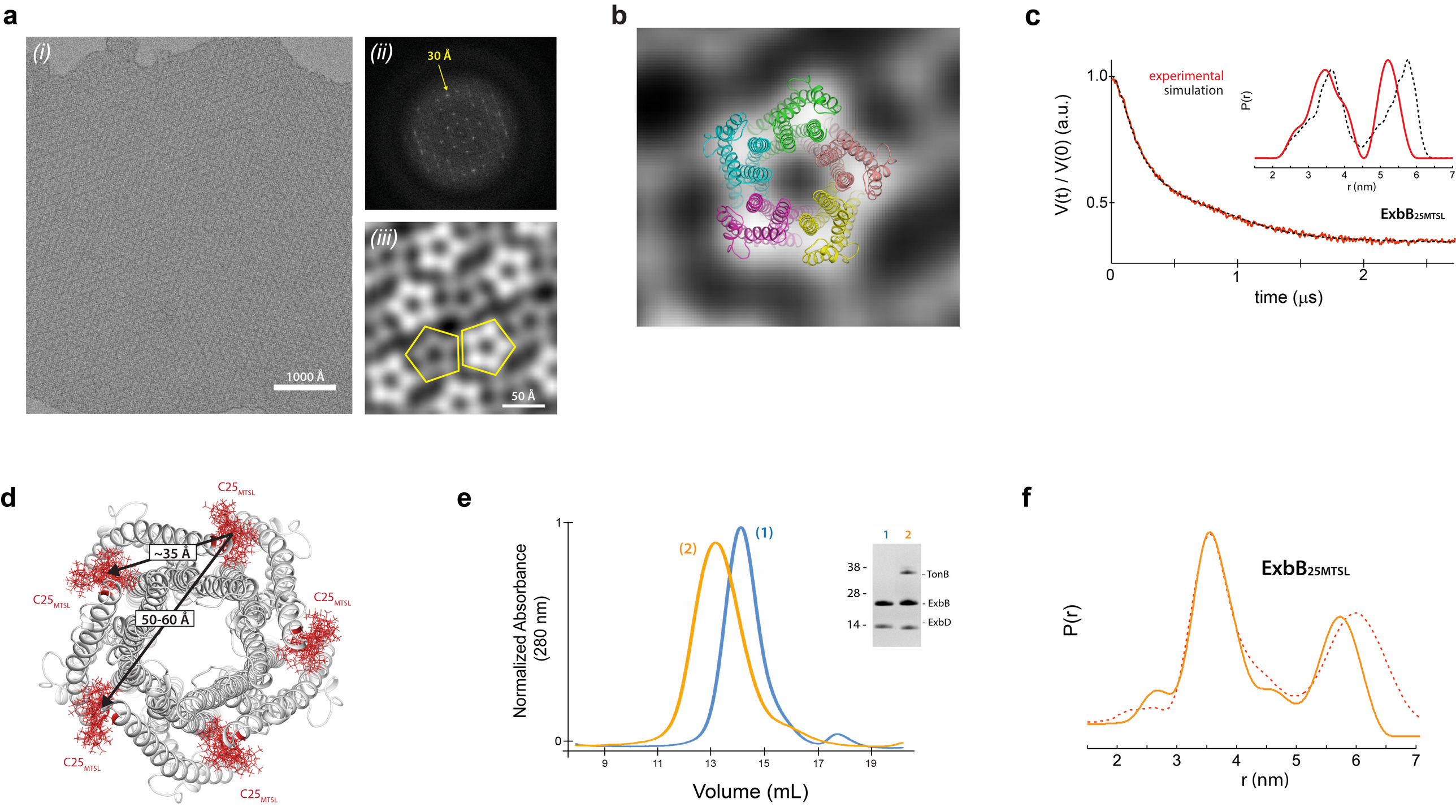
a
(i)
1000 Å
(ii)
30 Å
(iii)
50 Å
b
c
experimental
simulation
P(r)
r (nm)
ExbB25MTSL
V(t) / V(0) (a.u.)
time (μs)
d
C25MTSL
~35 Å
50-60 Å
e
Normalized Absorbance (280 nm)
Volume (mL)
(1)
(2)
1
2
38 -
28 -
14 -
TonB
ExbB
ExbD
f
ExbB25MTSL
P(r)
r (nm)

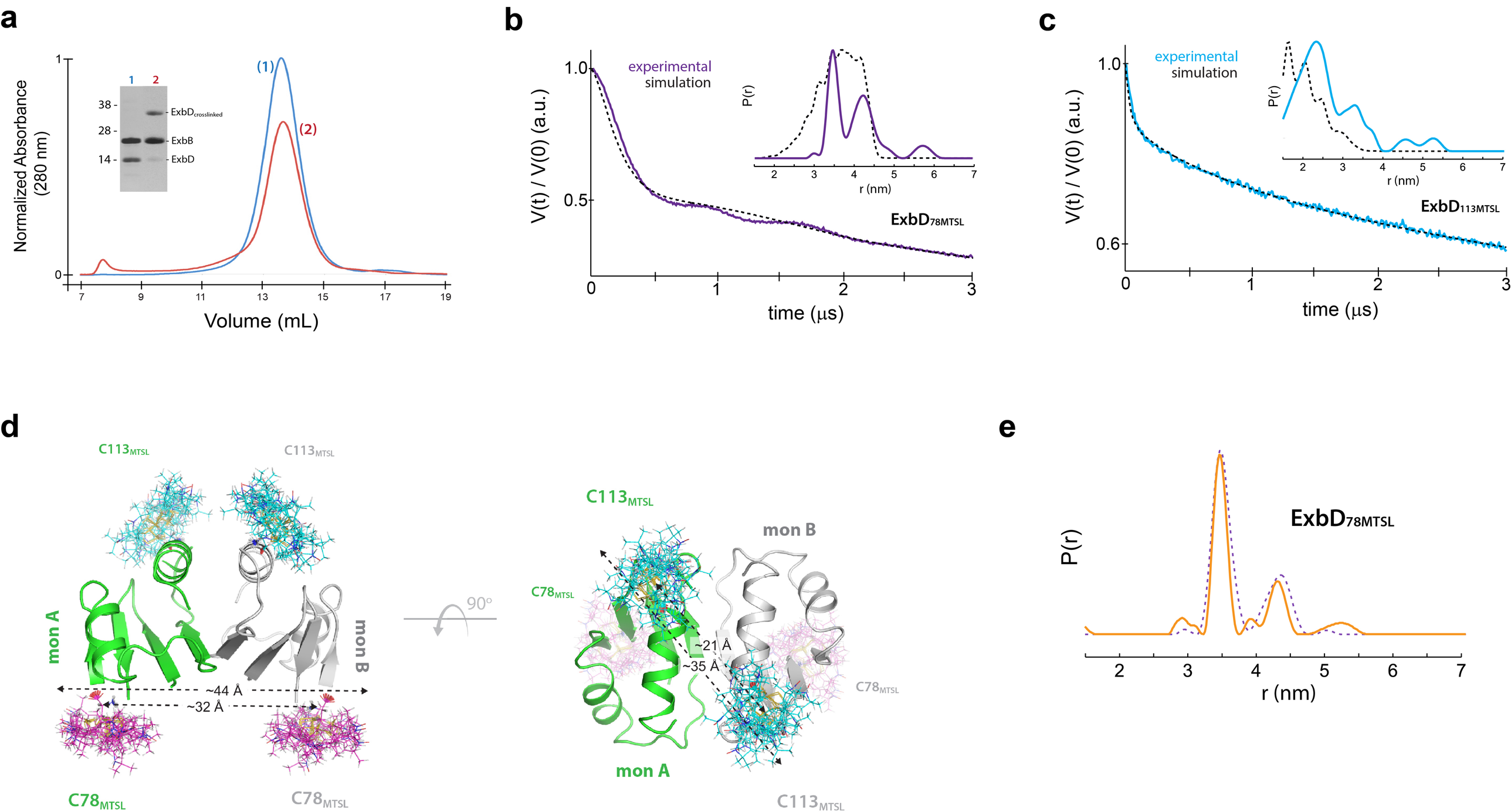
a
Normalized Absorbance (280 nm)
Volume (mL)
(1)
(2)
1
2
38 -
28 -
14 -
ExbD crosslinked
ExbB
ExbD
b
V(t) / V(0) (a.u.)
time (μs)
experimental
simulation
P(r)
r (nm)
ExbD78MTSL
c
V(t) / V(0) (a.u.)
time (μs)
experimental
simulation
P(r)
r (nm)
ExbD113MTSL
d
C113MTSL
C113MTSL
mon A
mon B
~44 Å
~32 Å
C78MTSL
C78MTSL
90°
C113MTSL
mon B
C78MTSL
~21 Å
~35 Å
C78MTSL
mon A
C113MTSL
e
P(r)
ExbD78MTSL
r (nm)

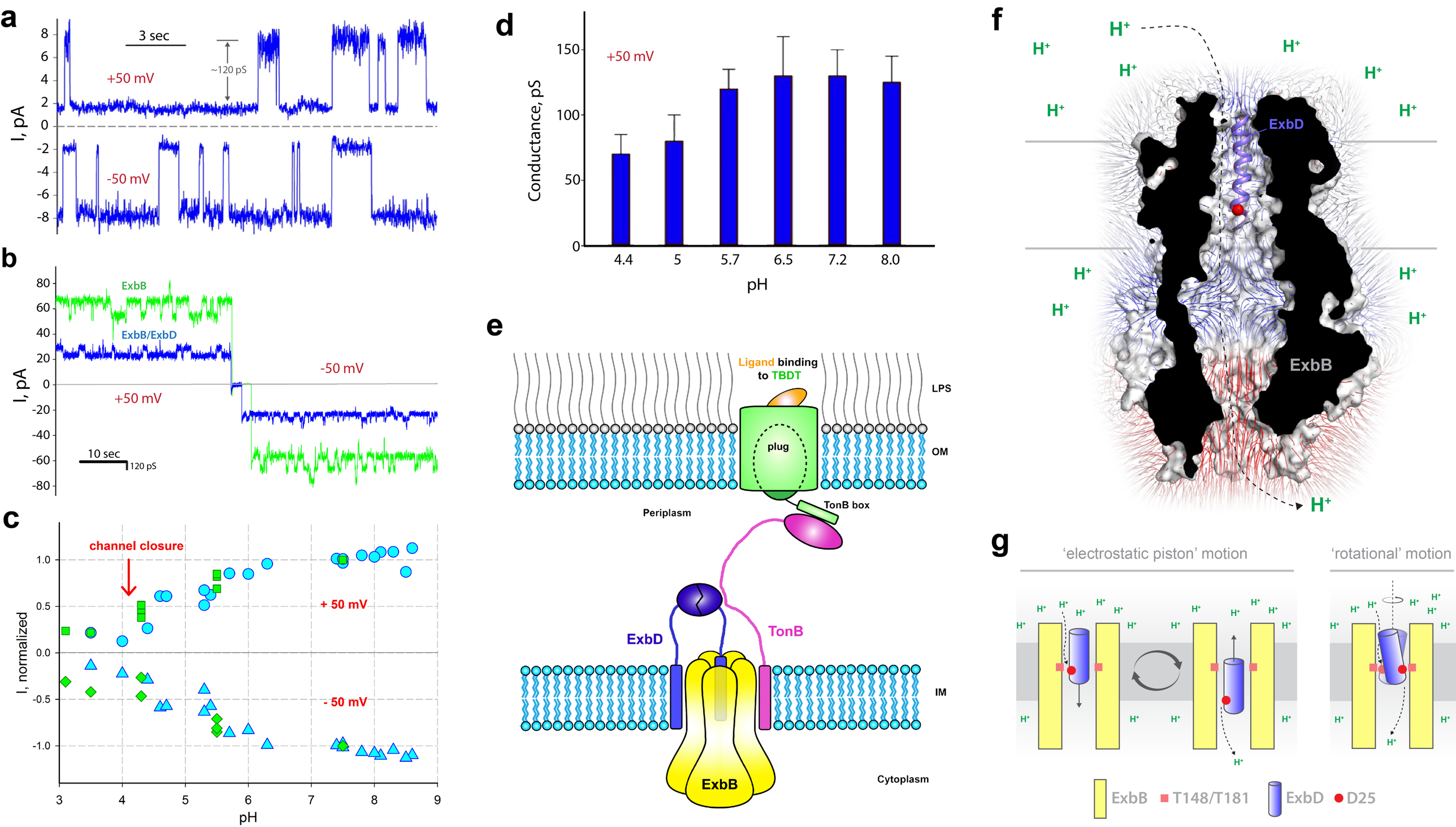
a
3 sec
~120 pS
+50 mV
-50 mV
I, pA
b
ExbB
ExbB/ExbD
-50 mV
+50 mV
10 sec
120 pS
I, pA
c
channel closure
+ 50 mV
- 50 mV
I, normalized
pH
d
+50 mV
Conductance, pS
pH
e
Ligand binding
to TBDT
LPS
plug
OM
Periplasm
TonB box
ExbD
TonB
IM
ExbB
Cytoplasm
f
ExbD
ExbB
H+
g
'electrostatic piston' motion
'rotational' motion
ExbB
T148/T181
ExbD
D25